Int J Fract (2010) 166:163–172
DOI 10.1007/s10704-010-9520-7

ORIGINAL PAPER

Fracture simulation of ferroelectrics based on the phase field continuum and a damage variable

Bai-Xiang Xu · David Schrade · Dietmar Gross · Ralf Mueller

Received: 16 December 2009 / Accepted: 7 June 2010 / Published online: 29 June 2010

Abstract Domain switching in the vicinity of a crack tip is known as one of the major aspects of local nonlinear behavior of ferroelectrics, and it plays an important role in the fracture behavior. In the present paper, a fracture model based on a phase field continuum and a damage variable is presented to study the fracture behavior of ferroelectrics and its interaction with the domain structures. In this model the energy of fracture is regularized by the damage variable. When the damage variable equals one, it represents undamaged material. In this case, the energy reduces to the phase field potential with the spontaneous polarization being an order parameter, and the system of equations becomes the same as that of a conventional phase field continuum. When the damage variable becomes zero, it represents a crack region, and the potential becomes the energy density stored in the crack medium. The evolution of the damage variable is governed by a Ginzburg-Landau type equation. In this way, the fracture model can simulate the fracture behavior such as crack growth, kinking and formation, with no a priori assumption on fracture criteria and predefined crack paths. The model is implemented in a 2D Finite Element Method in combination with implicit time integration and non-linear Newton iteration. As example, the fracture model is used to simulate the fracture of an edge crack in a ferroelectric single crystal under mechanical mode-I loading. In the simulation crack propagation, kinking and formation are observed. In particular, the results show the interaction between the domain structure evolution and the crack propagation.

Keywords Phase field simulation · Ferroelectric domain structure · Continuum fracture model · Crack propagation

The generous support by the Alexander von Humboldt Foundation is gratefully acknowledged.

B.-X. Xu (✉) · R. Mueller
Chair of Applied Mechanics, Department of Mechanical and Process Engineering,
TU Kaiserslautern, Kaiserslautern, Germany
e-mail: baxiaxu@rhrk.uni-kl.de

R. Mueller
e-mail: ram@rhrk.uni-kl.de

D. Schrade · D. Gross
Division of Solid Mechanics, Department of Civil Engineering and Geodesy, TU Darmstadt,
Darmstadt, Germany
e-mail: schrade@mechanik.tu-darmstadt.de

D. Gross
e-mail: gross@mechanik.tu-darmstadt.de

1 Introduction

Due to their large electro-mechanical coupling effects, high resolution and acceleration, ferroelectric ceramics are widely used in the application of e.g. actuators, sensors and transducers. It is known that in most cases the material has to perform at relatively high electric fields and mechanical loading, in order to achieve its

full electro-mechanical coupling effect. For example, the stresses induced in the ferroelectric actuators may reach up to 50 MPa, which is almost the strength of the material. On the other hand, the fracture toughness of ceramics is rather low (around $1\text{MPa}\sqrt{\text{m}}$). Hence, ferroelectric ceramics are intrinsically brittle and prone to fracture. Extensive studies on fracture of the material have been carried out, both theoretical and experimental. Recent reviews on this topic can be found in e.g. Zhang et al. (2002), Zhang and Gao (2004), Chen and Hasebe (2005), Schneider (2007) and the references cited therein. As it is shown in the literature, fracture of ferroelectrics is a complicated process, which can be influenced by a number of factors. In particular, experiments show that domain switching around the crack tip is one of the major aspects which induce local nonlinearity and therefore have a significant effect on fracture behavior of the material.

In the present paper a fracture model is developed to study the quasi-static fracture process of ferroelectrics and particularly its interaction with domain structures in the vicinity of a crack tip. The model is mainly based on two conceptions: (a) fracture via a regularized damage parameter and (b) a phase field continuum model for describing the ferroelectric domain switching. Features of the two conceptions are explained in the following.

In conventional fracture mechanics a crack is defined by its usually traction-free crack faces, and fracture is described by growth of the crack. However, the crack formation and growth in this work is described by a damage variable s. In doing so, the energy of fracture is regularized, in the way that $s = 1$ for the undamaged material and $s = 0$ for a crack region. In other words, the potential reduces to the potential for the undamaged material when $s = 1$, whereas the potential becomes the energy density stored in the crack medium when $s = 0$. It is important that the evolution of the damage variable is governed by a Ginzburg-Landau type equation. This damage variable theory enables the model to recapitulate the fracture behavior such as crack propagation, kinking and crack formation, with no a priori assumption on fracture criteria and predefined crack paths. Fundamental research on this type of continuum fracture model can be found e.g. in Kuhn and Mueller, Kuhn and Mueller (2008), Spatschek et al. (2006), Eastgate et al. (2002), Aranson et al. (2000), Bourdin et al. (2000), Francfort and Marigo (1998).

Second, a continuum phase field model for ferroelectric domain switching (Schrade et al. 2007; Mueller et al. 2007; Xu et al. 2009) is adopted for the undamaged material. When the damage variable $s = 1$, the potential coincides with the phase field potential proposed in Schrade et al. (2007), Mueller et al. (2007), Xu et al. (2009), and the system of equations correspondingly reduces to that presented there. By treating the spontaneous polarization as an order parameter subject to a Ginzburg-Landau type evolution equation, the phase field continuum is able to model the polarization switching and the domain structure under different electric/mechanical loadings and various boundary conditions. In fact, phase field methods have been used on the study of domain switching around stationary cracks in single ferroelectrics e.g. Song et al. (2007), Wang and Zhang (2007). By using the generalized configurational force as a fracture parameter, the phase field continuum was also applied to analyze the domain structure and its influence in cracked single crystal (Xu et al. 2010; Mueller et al. accepted).

It is noted that in the present fracture model no effort is needed for the issue of crack face boundary conditions. As it has been mentioned above, in the crack region ($s = 0$) the potential becomes the energy density stored in the crack medium. It means that the energy flowing into the crack has been taken into account in the model, and therefore no extra crack face boundary conditions need be considered. The material property of the crack medium can be chosen according to the specific working conditions, e.g. air, oil or water.

As a basic example, the fracture model implemented in 2D Finite Element Method (FEM) is used to simulate the fracture process of a semi-crack in a ferroelectric single crystal under mechanical mode-I loading. Since a mono-domain structure may not be a stable configuration for a cracked single crystal even before the mechanical loading, the first step of the simulation is to obtain the initial equilibrium configuration. Results show that energy minimization leads to a diffusion of the damage variable s and a new self-equilibrium domain structure. Starting from this initial equilibrium configuration, the cracked single crystal is then prescribed with a tensile loading. During the fracture process, results for the damage variable and the corresponding domain structures are documented, and crack propagation, kinking and crack formation are numerically observed.

2 Fracture model based on the phase field continuum and a damage variable

2.1 The regularized energy via a damage variable

In the formulation of fracture in ferroelectrics, a damage variable $s \in [0, 1]$ is introduced to indicate the crack situation. In principle, it represents the crack region when the damage variable becomes zero, and undamaged material when the damage variable equals one. In this way, the energy of fracture can be regularized. For the ferroelectrics a regularized energy expression is given as follows,

$$\psi = \underbrace{s^2 H + (1-s^2)\left(\frac{1}{2}\boldsymbol{\varepsilon} : (\mathbf{C}_c\boldsymbol{\varepsilon}) - \frac{1}{2}\mathbf{E}\cdot(\mathbf{A}_c\mathbf{E})\right)}_{E_b} + \underbrace{\frac{G_c}{4\lambda_c}(1-s^2) + G_c\lambda_c \|\mathrm{grad} s\|^2}_{E_s} . \tag{1}$$

Note that the energy is split into two parts: the energy stored in the bulk E_b and the energy stored in the crack surface E_s. In the bulk energy, $H = H(\boldsymbol{\varepsilon}, \mathbf{E}, \boldsymbol{P}, \mathrm{grad}\boldsymbol{P})$ is the phase field potential for undamaged ferroelectric solid, with $\boldsymbol{\varepsilon}$ being the strain, $\boldsymbol{E}$ the electric field and $\boldsymbol{P}$ the spontaneous polarization. Details on the phase field potential H can be found in the following subsection. Further, $\boldsymbol{C}_c$ and $\boldsymbol{A}_c$ are the stiffness tensor and the dielectric tensor of the medium (e.g. air, water or oil) inside the crack, respectively. The stiffness of the crack medium $\boldsymbol{C}_c$ is usually negligible, compared with the stiffness of ceramics. It is apparent that the bulk energy E_b turns to be the phase field potential H when $s = 1$, whereas the bulk energy E_b becomes the energy stored in the crack medium when $s = 0$. Following the idea of phase field theories, the surface energy E_s is assumed to be dependent on the gradient of the damage variable s and certain polynomial terms. The parameters G_c and λ_c are the specific energy and the width of the transition zone where s changes from 0 to 1. Furthermore, the damage variable s is assumed to follow the Ginzburg-Landau type evolution equation

$$\dot{s} = -M_c\frac{\delta\psi}{\delta s} = -M_c\left(\frac{\partial E_b}{\partial s} - \frac{G_c}{2\lambda_c}s - 2G_c\lambda_c\Delta s\right), \tag{2}$$

where M_c is the mobility parameter, and Δ is the Laplace operator. It is noted that the present fracture model is a generalization of the phase field fracture models, e.g. Kuhn and Mueller, Kuhn and Mueller (2008), Spatschek et al. (2006), Eastgate et al. (2002), Aranson et al. (2000), Bourdin et al. (2000), Francfort and Marigo (1998), from elastic material to ferroelectrics ceramics.

2.2 Phase field potential for undamaged ferroelectrics

Ferroelectric solids are known to exhibit a domain structure (domains separated by domain walls), which is intrinsically the results of the inhomogeneous distribution of the spontaneous polarization $\boldsymbol{P}$ in the material. According to the continuum phase field model (Schrade et al. 2007, Mueller et al. (2007), Xu et al. (2009)), the ferroelectric behavior can be simulated by introducing the spontaneous polarization $\boldsymbol{P}$ as an order parameter. The energy in a ferroelectric solid is then given by a phase field potential, which consists of three parts,

$$H = H^{\mathrm{ent}} + H^{\mathrm{sep}} + H^{\mathrm{int}} . \tag{3}$$

In the last equation H^{ent} is the classical electric enthalpy, and H^{sep} is the domain separation energy which is mainly responsible for the formation of domains, and H^{int} is the interface energy which takes into account the energy stored in the domain walls. Their representations are given by

$$H^{\mathrm{ent}} = \frac{1}{2}(\boldsymbol{\varepsilon} - \boldsymbol{\varepsilon}^0) : [\boldsymbol{C}(\boldsymbol{\varepsilon} - \boldsymbol{\varepsilon}^0)] - (\boldsymbol{\varepsilon} - \boldsymbol{\varepsilon}^0) : [\boldsymbol{b}^{\mathrm{T}}\boldsymbol{E}] - \frac{1}{2}\boldsymbol{E}\cdot(\boldsymbol{A}\boldsymbol{E}) - \boldsymbol{P}\cdot\boldsymbol{E}, \tag{4}$$

$$H^{\mathrm{sep}} = \kappa_{\mathrm{s}}\frac{G}{\lambda}\left[1 + \frac{a_1}{P_0^2}\left(P_1^2+P_2^2\right) + \frac{a_2}{P_0^4}\left(P_1^4 + P_2^4\right) + \frac{a_3}{P_0^4}P_1^2P_2^2 + \frac{a_4}{P_0^6}\left(P_1^6 + P_2^6\right)\right], \tag{5}$$

$$H^{\mathrm{int}} = \kappa_{\mathrm{i}}\frac{G\lambda}{P_0^2}\|\mathrm{grad}\boldsymbol{P}\|^2 , \tag{6}$$

where Eq. (5) is tailored for the 2D case. In the last equations G and λ are the specific energy and the width of a 180° domain wall, respectively. The coefficients κ_s and κ_i are used to calibrate the two parameters. Based on the investigation of a 180° domain wall, we take $\kappa_s = 0.70$ and $\kappa_i = 0.17$ (For details readers are referred to Schrade et al. (2009, 2010)). In Eq. (5) P_1 and P_2 are

the Cartesian components of the spontaneous polarization $\boldsymbol{P}$ and a_i $(i = 1, \ldots, 4)$ are parameters which specify the energy landscape, i.e. determine the energy for domains to switch from one variant to another. The domain separation energy achieves local minima at the four variants $(\pm P_0, 0)$ and $(0, \pm P_0)$. In Eq. (4) $\boldsymbol{C}$ is the elastic stiffness tensor, $\boldsymbol{b}$ the piezoelectric tensor, $\boldsymbol{A}$ the dielectric tensor, and $\boldsymbol{\varepsilon}^0$ the spontaneous strain. It should be noted that the spontaneous strain $\boldsymbol{\varepsilon}^0$ and the piezoelectric tensor $\boldsymbol{b}$ depend on the spontaneous polarization $\boldsymbol{P}$, see e.g. Kamlah (2001),

$$\boldsymbol{\varepsilon}^0(\boldsymbol{P}) = \frac{3}{2}\varepsilon_0 \frac{\|\boldsymbol{P}\|}{P_0}\left(\boldsymbol{e}\otimes\boldsymbol{e} - \frac{1}{3}\mathbf{1}\right), \tag{7}$$

$$b_{kij}(\boldsymbol{P}) = \frac{\|\boldsymbol{P}\|}{P_0}\Big\{ b_{\parallel} e_i e_j e_k + b_{\perp}(\delta_{ij} - e_i e_j)e_k + b_{=}\frac{1}{2}\left[(\delta_{ki} - e_k e_i)e_j + (\delta_{kj} - e_k e_j)e_i\right]\Big\}, \tag{8}$$

where $\boldsymbol{e} = \boldsymbol{P}/\|\boldsymbol{P}\|$ is the unit vector along $\boldsymbol{P}$, and $\varepsilon_0, b_{\parallel}, b_{\perp}, b_{=}$ are material parameters. In Eq. (8) index notation has been used for compact notation.

Different from that in the continuum phase field model (Schrade et al. 2007; Mueller et al. 2007; Xu et al. 2009), the evolution equation of the order parameter $\boldsymbol{P}$ is given by the variation of the energy ψ, instead of the phase field potential H. That is

$$\dot{\boldsymbol{P}} = -M\frac{\delta\psi}{\delta\boldsymbol{P}} = -s^2 M\frac{\delta H}{\delta\boldsymbol{P}} = -s^2 M\left(\frac{\partial H}{\partial\boldsymbol{P}} - 2\kappa_1\frac{G\lambda}{P_0^2}\Delta\boldsymbol{P}\right), \tag{9}$$

in which M is the mobility parameter of the domain wall. In this way, the evolution equation involves also the damage variable s, and then the model can recapitulate the interaction of the domain structure and the crack propagation.

2.3 Field equations

Suppose that the electro-mechanical fields evolve relatively slow compared to the speed of light and sound so that the fields can be considered as quasi-static. Thus the stress $\boldsymbol{\sigma}$ fulfills the equilibrium condition, and the electric displacement $\boldsymbol{D}$ is governed by Gauß' law,

$$\operatorname{div}\boldsymbol{\sigma} = \mathbf{0}, \quad \operatorname{div}\boldsymbol{D} = 0\,. \tag{10}$$

where the stress and the electric displacement are given by the following constitutive equations

$$\boldsymbol{\sigma} = \frac{\partial\psi}{\partial\boldsymbol{\varepsilon}} = s^2\left[\boldsymbol{C}(\boldsymbol{\varepsilon} - \boldsymbol{\varepsilon}^0) - \boldsymbol{b}^{\mathrm{T}}\boldsymbol{E}\right] + (1-s^2)\boldsymbol{C}_c\boldsymbol{\varepsilon}, \tag{11}$$

$$\boldsymbol{D} = -\frac{\partial\psi}{\partial\boldsymbol{E}} = s^2\left[\boldsymbol{b}(\boldsymbol{\varepsilon}-\boldsymbol{\varepsilon}^0)+\boldsymbol{A}\boldsymbol{E}+\boldsymbol{P}\right]+(1-s^2)\boldsymbol{A}_c\boldsymbol{E}. \tag{12}$$

The strain $\boldsymbol{\varepsilon}$ and the electric field $\boldsymbol{E}$ are defined as follows

$$\boldsymbol{\varepsilon} = \frac{1}{2}\left(\operatorname{grad}\boldsymbol{u} + \operatorname{grad}^{\mathrm{T}}\boldsymbol{u}\right), \quad \boldsymbol{E} = -\operatorname{grad}\varphi\,, \tag{13}$$

where $\boldsymbol{u}$ is the displacement, and φ the electric potential. Two types of mechanical boundary conditions are usually considered

$$\boldsymbol{\sigma}\boldsymbol{n} = \boldsymbol{t}^*, \quad \boldsymbol{u} = \boldsymbol{u}^*, \tag{14}$$

where $\boldsymbol{n}$ is the outward normal vector at the boundary, and $\boldsymbol{t}^*$ and $\boldsymbol{u}^*$ are the prescribed surface tractions and displacements, respectively. Possible electric boundary conditions are

$$\boldsymbol{D}\cdot\boldsymbol{n} = -Q^*, \quad \varphi = \varphi^*, \tag{15}$$

where Q^* and φ^* are the applied surface charge density and the applied electric potential, respectively.

3 Finite element implementation

The damage model presented in the previous section is implemented in the 2D Finite Element Method (FEM). The discretization is done by four-node bi-linear plane elements. For more details, the reader is referred to standard textbooks on Finite Element Methods, e.g. Hughes (2000). In the implementation the displacement $\mathbf{u}$, the electric potential φ, and the spontaneous polarization $\mathbf{P}$, and the damage variable s are taken as the nodal degrees of freedom. Thus, each node has six degrees of freedom, namely

$$\underline{\mathbf{d}}^I = \left[\, u_1^I \;\; u_2^I \;\; \varphi^I \;\; P_1^I \;\; P_2^I \;\; s^I \,\right]^T, \tag{16}$$

where the superscript I indicates the element node, and the underbar in this paper denotes a matrix notation. Corresponding to the strong forms Eqs. (10), (9) and (2), the following four weak forms are formulated for the implementation, respectively,

$$
\begin{aligned}
&-\int_{\mathscr{B}} \boldsymbol{\sigma} : \operatorname{grad} \boldsymbol{\eta}_u \, dV = 0 \,, \\
&-\int_{\mathscr{B}} \mathbf{D} \cdot \operatorname{grad} \eta_\varphi \, dV = 0 \,, \\
&-\int_{\mathscr{B}} \Bigg[\left(\frac{1}{M} \dot{\mathbf{P}} + s^2 \frac{\partial H}{\partial \mathbf{P}} \right) \cdot \boldsymbol{\eta}_{\mathbf{P}} \\
&\qquad + 2G \, \lambda \, s^2 \operatorname{grad} \mathbf{P} : \operatorname{grad} \boldsymbol{\eta}_P \Bigg] dV = 0, \\
&-\int_{\mathscr{B}} \Bigg[\left(\frac{1}{M_c} \dot{s} + \frac{\partial \psi}{\partial s} \right) \eta_s \\
&\qquad + 2G_c \, \lambda_c \operatorname{grad} s \cdot \operatorname{grad} \eta_s \Bigg] dV = 0,
\end{aligned}
\tag{17}
$$

where η_u, η_φ, η_P and η_s are the test functions. Shape functions are introduced to interpolate $\mathbf{u}$, φ, $\mathbf{P}$, s, $\dot{\mathbf{P}}$, $\dot{s}$ and the test functions,

$$
\begin{aligned}
\underline{\mathbf{u}} &= \sum_I N_u^I \, \underline{\mathbf{u}}^I \,, \quad \varphi = \sum_I N_\varphi^I \, \varphi^I \,, \\
\underline{\mathbf{P}} &= \sum_I N_P^I \, \underline{\mathbf{P}}^I \,, \quad s = \sum_I N_s^I \, s^I \,,
\end{aligned}
\tag{18}
$$

$$
\begin{aligned}
\underline{\boldsymbol{\eta}}_u &= \sum_I N_u^I \, \underline{\boldsymbol{\eta}}_u^I, \; \eta_\varphi = \sum_I N_\varphi^I \, \eta_\varphi^I \,, \\
\underline{\boldsymbol{\eta}}_P &= \sum_I N_P^I \, \underline{\boldsymbol{\eta}}_P^I \,, \quad \eta_s = \sum_I N_s^I \, \eta_s^I \,,
\end{aligned}
\tag{19}
$$

$$
\dot{\underline{\mathbf{P}}} = \sum_I N_P^I \, \dot{\underline{\mathbf{P}}}^I \,, \qquad \dot{s} = \sum_I N_s^I \, \dot{s}^I \,. \tag{20}
$$

Making use of Eq. (13), the strain and the electric field can be expressed by the following matrix notation

$$
\underline{\varepsilon} = \sum_I \underline{\mathbf{B}}_u^I \, \underline{\mathbf{u}}^I \,, \quad \underline{\mathbf{E}} = -\sum_I \underline{\mathbf{B}}_\varphi^I \, \varphi^I \,, \tag{21}
$$

where

$$
\underline{\mathbf{B}}_u^I = \begin{bmatrix} N_{u,x}^I & 0 \\ 0 & N_{u,y}^I \\ N_{u,y}^I & N_{u,x}^I \end{bmatrix} \,, \quad \underline{\mathbf{B}}_\varphi^I = \begin{bmatrix} N_{\varphi,x}^I \\ N_{\varphi,y}^I \end{bmatrix} \,. \tag{22}
$$

The gradient of the polarization and the damage variable can also be interpolated as following

$$
\operatorname{grad} \underline{\mathbf{P}} = \sum_I \underline{\mathbf{B}}_P^I \, \underline{\mathbf{P}}^I \,, \quad \operatorname{grad} s = \sum_I \underline{\mathbf{B}}_s^I \, s^I \,, \tag{23}
$$

in which

$$
\underline{\mathbf{B}}_P^I = \begin{bmatrix} N_{P,x}^I & 0 \\ 0 & N_{P,y}^I \\ N_{P,y}^I & 0 \\ 0 & N_{P,x}^I \end{bmatrix} \,, \quad \underline{\mathbf{B}}_s^I = \begin{bmatrix} N_{s,x}^I \\ N_{s,y}^I \end{bmatrix} \tag{24}
$$

Inserting the FEM approximation (18)–(24) into the weak forms (17), one obtains the element residuals $\underline{\mathbf{R}}^I = \left(\underline{\mathbf{R}}_\sigma^I, \; R_D^I, \; \underline{\mathbf{R}}_P^I, \; R_s^I \right)^T$ with

$$
\begin{aligned}
\underline{\mathbf{R}}_\sigma^I &= -\int_{\mathscr{B}^e} \underline{\mathbf{B}}_u^{I\,T} \, \underline{\boldsymbol{\sigma}} \, dV, \\
R_D^I &= -\int_{\mathscr{B}^e} \underline{\mathbf{B}}_\varphi^{I\,T} \, \underline{\mathbf{D}} \, dV \,, \\
\underline{\mathbf{R}}_P^I &= -\int_{\mathscr{B}^e} \Bigg[\left(\frac{1}{M} \dot{\underline{\mathbf{P}}} + s^2 \frac{\partial H}{\partial \mathbf{P}} \right) N_P^I \\
&\qquad + 2G \, \lambda \, s^2 \underline{\mathbf{B}}_P^{I\,T} \operatorname{grad} \underline{\mathbf{P}} \Bigg] dV, \\
R_s^I &= -\int_{\mathscr{B}^e} \Bigg[\left(\frac{1}{M_c} \dot{s} + \frac{\partial \psi}{\partial s} \right) N_s^I \\
&\qquad + 2G_c \, \lambda_c \, \underline{\mathbf{B}}_s^{I\,T} \operatorname{grad} s \Bigg],
\end{aligned}
\tag{25}
$$

in which the stress and the electric displacement are given in the following matrix notation in use of Eq. (11) and (12)

$$
\underline{\boldsymbol{\sigma}} = s^2 \left[\mathbb{C} (\underline{\boldsymbol{\varepsilon}} - \underline{\boldsymbol{\varepsilon}}^0) - \mathbb{b}^T \underline{\mathbf{E}} \right] + (1 - s^2) \underline{\boldsymbol{C}}_c \underline{\varepsilon}, \tag{26}
$$

$$
\underline{\mathbf{D}} = s^2 \left[\mathbb{b} (\underline{\boldsymbol{\varepsilon}} - \underline{\boldsymbol{\varepsilon}}^0) + \underline{\mathbf{A}} \, \underline{\mathbf{E}} + \underline{\mathbf{P}} \right] + (1 - s^2) \underline{\boldsymbol{A}}_c \underline{\mathbf{E}} \,. \tag{27}
$$

Assembly of the element residuals gives the global residual vector $\underline{\mathbf{R}}$, and then numerical strategies are needed to solve $\underline{\mathbf{R}} = \mathbf{0}$. Since this assembly process is a standard procedure in FEM, it is not explained in detail here. It can be seen that this set of equations is time-dependent and nonlinear. The time dependence of the residual is treated by an implicit time integration method. The rates of the global nodal values $\underline{\mathbf{d}}$ are discretized in time by

$$
\dot{\underline{\mathbf{d}}} \approx \frac{\underline{\mathbf{d}}_{n+1} - \underline{\mathbf{d}}_n}{\Delta t} \,, \tag{28}
$$

where the subscript n denotes the time step. Then the time-dependent residual $\underline{\mathbf{R}}(\underline{\mathbf{d}}, \dot{\underline{\mathbf{d}}})$ is given as

$$
\underline{\mathbf{R}} = \underline{\mathbf{R}} \left(\underline{\mathbf{d}}_{n+1}, \frac{\underline{\mathbf{d}}_{n+1} - \underline{\mathbf{d}}_n}{\Delta t} \right) = \mathbf{0} \,. \tag{29}
$$

Due to the nonlinearities in $\underline{\mathbf{R}}$, this implicit representation sets up a nonlinear system of equations for $\underline{\mathbf{d}}_{n+1}$. A Newton iteration is used to solve the nonlinear equations. The derivatives of the residual with respect to the degrees of freedom are given as

$$
\underline{\mathbf{K}}^{IJ} = -\frac{\partial \underline{\mathbf{R}}^I}{\partial \underline{\mathbf{d}}^J} \,, \quad \underline{\mathbf{D}}^{IJ} = -\frac{\partial \underline{\mathbf{R}}^I}{\partial \dot{\underline{\mathbf{d}}}^J} \,. \tag{30}
$$

From the implicit time integration, the tangent matrix of the Newton scheme is obtained as

$$\underline{\mathbf{S}}^{IJ} = \underline{\mathbf{K}}^{IJ} + \frac{1}{\Delta t}\underline{\mathbf{D}}^{IJ}. \tag{31}$$

According to the model and the numerical schemes stated above, a new user element was developed in the FEAP (the Finite Element Analysis Program).

4 Numerical results

As an illustrative example, quasi-static crack propagation in a ferroelectric single crystal subject to mode-I mechanical loading is investigated under the condition of plane strain deformation. In the simulations homogeneous Neumann boundary conditions are assumed for the order parameter $\boldsymbol{P}$ and the damage variable s, so that there is no flux of the related variables on the boundary. The material parameters for the undamaged region mimic piezoelectric material, and the dielectric constant for the crack region is taken from the air. For the numerical reasons, we assume that air also has the stiffness constants, but they are significantly smaller than those of ceramics. Based on the results on the ferroelectric bulk, the phase field parameters are taken as follows: $M = 10^7 \mathrm{A/(Vm)}$, $G = 1.83 \times 10^{-2} \mathrm{J/m^2}$ and $\lambda = 1.28 \times 10^{-7} \mathrm{m}$, while the parameters related to the crack evolution are $M_c = 1.0 \times 10^6\, \mathrm{m^2/(Ns)}$, $G_c = 10.0\, \mathrm{J/m^2}$ and $\lambda_c = 2.5 \times 10^{-7} \mathrm{m}$. The mobility parameters M and M_c are chosen such that the time scale of the domain structure evolution is comparable to the time scale of the crack propagation.

The setup for the numerical example is illustrated in Fig. 1. A rectangular single crystal ($1\mu\mathrm{m} \times 2\mu\mathrm{m}$) with downward initial polarization is prescribed with a starting crack and then with a mode-I tensile loading σ_0. The calculations consist of two steps: (1) A relaxation step is first calculated on the cracked single crystal with initially downward polarization, under charge-free and stress-free boundary conditions; (2) Starting from the relaxed configuration, the cracked single crystal is perscribed with a tensile loading at the top and the bottom, while the electrical boundary conditions remain charge-free. The results for each step are explained in the following subsections. In order to avoid the rigid body movement, the bottom left corner is fixed in both the x and y directions, and the bottom right corner is fixed in y direction. In the simulation uniform finite element meshes were used, with the mesh size smaller than the length parameters λ and fine enough to take into account the singularity at the crack tip.

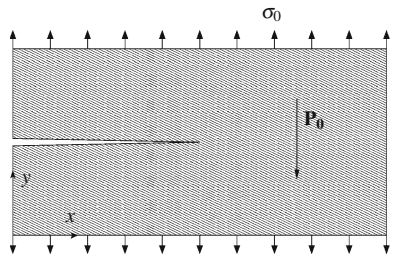

Fig. 1 Numerical setup

4.1 Initial equilibrium state

At the first step of the calculation the initial crack is prescribed by setting initial values for s: zero at the crack position and one for the remaining part. The initial configuration of the calculation is shown in Fig. 2. After the initial crack is introduced into the single crystal, the original mono-domain structure is not stable any more. As a result of energy minimization, calculation leads to a diffusion of the transition zone in the field of the damage variable s and a new self-equilibrium domain structure, depicted in Fig. 3 a, b, respectively. Even though the polarization at the region in front of the crack remains in the initial downward direction, the mono-domain structure breaks down above and below the crack. It is seen that the polarization along the crack surfaces is switched by 90° (above/below the crack face polarizations pointing to the right/left), due

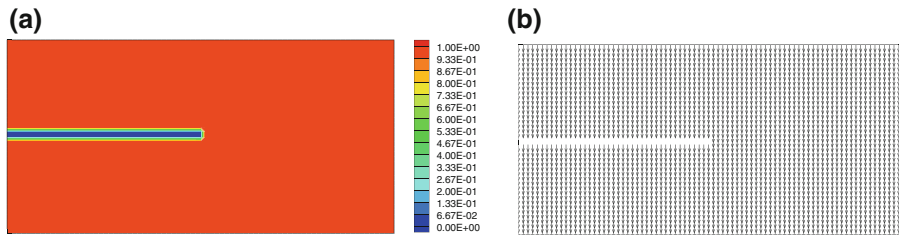

Fig. 2 Initial configuration: **a** Contour plot for the damage variable s, **b** Polarization

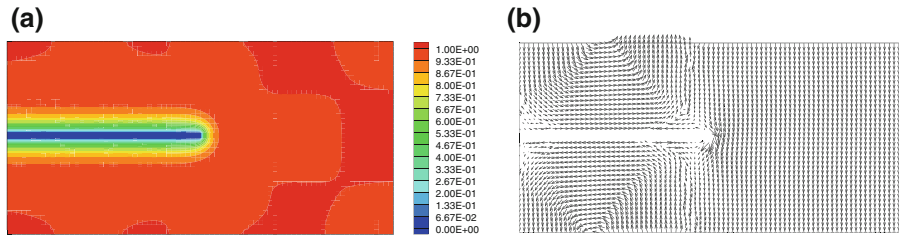

Fig. 3 Initial equilibrium configuration: **a** Contour plot for the damage variable s, **b** Polarization

to the presence of the crack surfaces. However, in the regions on the very left of the specimen, the charge-free boundary conditions keep the polarizations in the initial downward direction. This gives rise to two 90° domain walls, one at the top left and one at the bottom left, respectively. Between these 90° domain walls and the intact left region, there is a transition zone where polarizations are switched by 180°. Therefore another 90° domain wall and one 180° domain wall are formed, appearing symmetrically above and below the crack tip. Furthermore, two asymmetric sub-domains confined by 90° domain walls and the crack surfaces (above/below the crack face polarizations pointing to the right/left) are noticeable at the crack tip.

4.2 Mode-I crack propagation

Starting from the stationary configuration shown in Fig. 3, the cracked single crystal is subjected to a tensile loading in the y direction at the top and the bottom. The magnitude of the tensile loading σ_0 steadily increases with time, so that at each time step the domain structure has enough time to reach its quasi-static equilibrium configuration. By using the material parameters given above, crack growth is observed when the tensile loading reaches about 42.8 MPa. Figure 4 shows the snap shots of the damage variable and the polarization at five major situations during the cracking process. According to the time sequence, the five situations are cited as Situation I-V, respectively.

Situation I, i.e. Fig. 4 (a) and (b), is the moment right before the crack starts to propagate. In comparison with the initial equilibrium configuration in Fig. 3, apparent changes can be found in the domain structure. The sub-domains with horizontal polarization in the initial equilibrium configuration grow larger now. The result indicates that before the crack actually starts to move, the material tries first to reorient the domain structure in order to minimize the energy. However, due to the limit of the domain structure relaxation, the crack has to propagates eventually, which is shown in the next situation.

At the situation II, i.e. Fig. 4 (c) and (d), it is seen that the prescribed crack propagates straight forward for a certain distance. As it is shown in the contour plot of the damage variable, new crack surfaces are created, Simultaneously, the polarization along the new crack surface is switched by 90°. Even though the shape of the domain structure remains similar to the previous situation in Fig. 4 (b), the position of the domain walls stretches to follow the moving crack tip. What can also be noticed is that the symmetry of the configuration starts to break down, which gives rise to the turning of the crack path in the next step.

It is observed at the situation III that the crack kinks and propagates to the left, see Fig. 4 (e). The angle between the previous propagating direction and the new one is around 60°. In the domain structure Fig. 4 (f), a domain wall is observed above the crack turning point. This domain wall triggers further propagation of the kinked crack.

At the situation IV it is seen that the crack continues to turn until the crack propagation direction becomes upward. Till this point, the direction of the propagation is turned up to 90°, see Fig. 4 (g). At the same time, a crack formation is observed on the surface over the crack tip where the domain wall ends. As it is shown at the situation V Fig. 4 (i), the previous crack and the new initiated crack propagate through the domain wall and finally coalesce at a certain point. From the situation III on, the main part of the domain structure remains similar, except that modifications appear at the moving crack tip and that the polarization locally switches so that it more or less realigns parallel to the newly created crack surface.

5 Concluding remarks

In the present paper a model is proposed for the study of fracture in ferroelectrics and its interaction with the

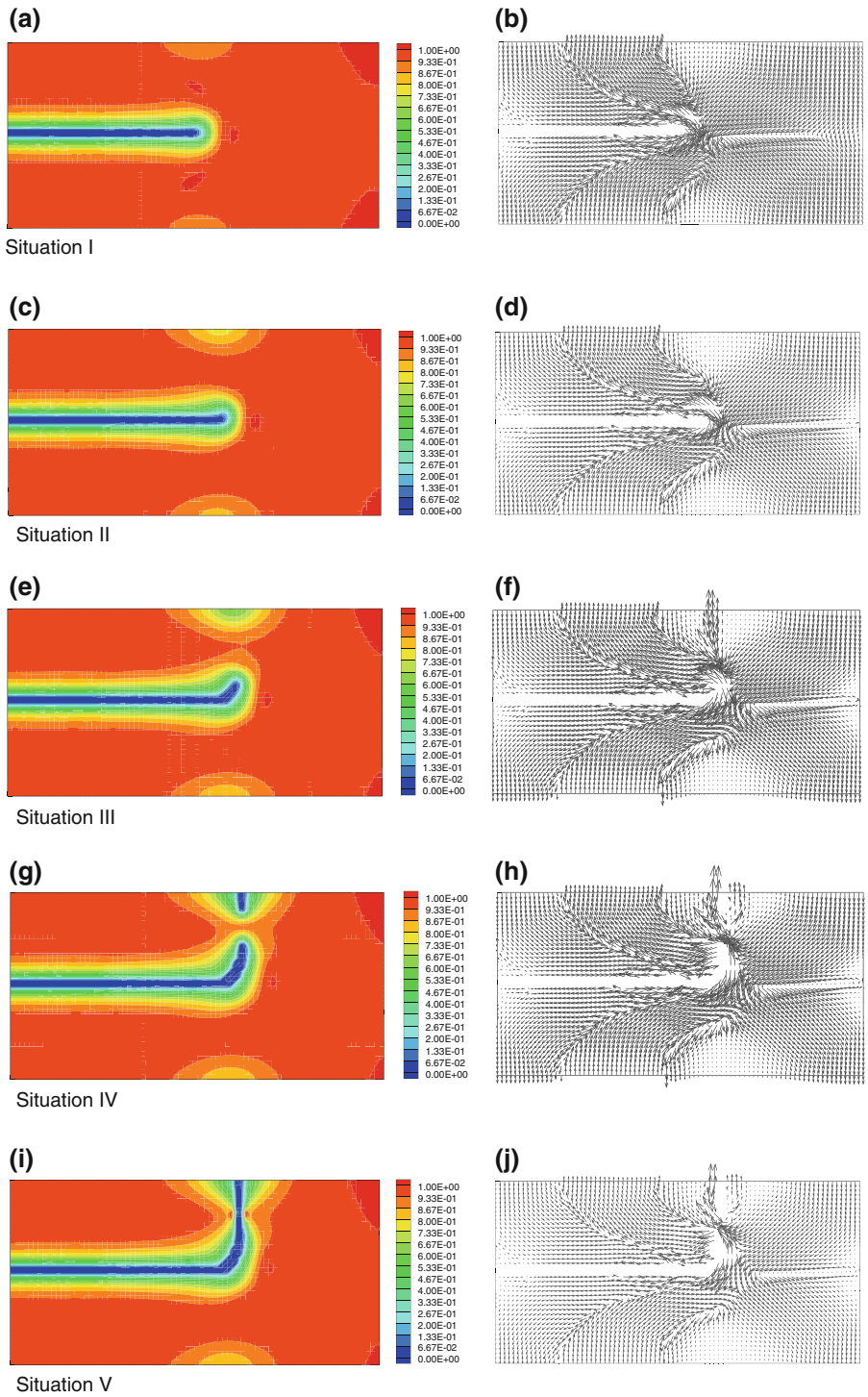

Fig. 4 Mode-I crack propagation: Damage variable, a → c → e → g → i; Polarization, b → d → f → h → j

domain switching in the material. The model is mainly based on the damage variable $s \in [0, 1]$ governed by a Ginzburg-Landau type equation and the previous continuum phase field model for ferroelectric domain switching (Schrade et al. 2007; Mueller et al. 2007; Xu et al. 2009).

In the numerical example, simulation is first carried out to achieve the domain structure at the initial self-equilibrium state. After a single crystal is prescribed with an initial crack (before the tensile loading is applied), the original mono-domain structure evolves into a new stationary configuration as a result of energy minimization. The new stationary domain structure adapts itself to the initial crack surface and the boundary conditions.

Then domain structures are documented for different situations during the fracture under a mode-I loading. The results show that before the crack starts to propagate, the material tries first to reorient the domain structure in order to minimize the energy. When the domain structure relaxation cannot satisfy the energy release requirement, the crack starts to propagate. During the propagation, the domain structure evolves with the crack propagation and adjusts itself to the new created crack surfaces. It is also numerically observed that the direction of the crack propagation can be altered in the presence of a domain wall, and that crack initiation can be triggered on the surface where domain wall ends.

In the model both the damage variable s and the order parameter $\boldsymbol{P}$ are subject to time evolution equations of the Ginzburg-Landau type, and hence two mobility parameters are introduced: M_c for the damage variable and M for the polarization. The parameter M_c should be related to the crack velocity, and the parameter M is relevant for the description of the domain structure. But in terms of exact values, both of them are usually unknown, even for standard commercial piezoelectric materials. As a test, the mobility parameters M and M_c in the example are chosen such that the time scale of the domain structure evolution is comparable to the time scale of the crack propagation. For more realistic simulations, parameter identification based on experiments is needed.

It is noted that the fracture model does not distinguish the energy between the tensile and compression cases. Therefore crack may be equally possible under the compression state as under the tensile state. Besides the presence of the domain wall, this may also be part of the reason for the formation of a new crack on the top of the specimen in the simulation. To avoid the problem in the compression state, one can replace the stress tensor by its deviatoric part in the fracture energy, i.e. Eq. (1). This is not yet considered in the present work. Meanwhile, more quantitative investigations of the fracture properties of ferroelectrics, especially the influence of applied electric fields, will be considered in the future.

References

Aranson IS, Kalatsky VA, Vinokur VM (2000) Continuum field description of crack propagation. Phys Rev Lett 85(1):118–121

Bourdin B, Francfort GA, Marigo JJ (2000) Numerical experiments in revisited brittle fracture. J Mech Phys Solids 48:797–826

Chen YH, Hasebe N (2005) Current understanding on fracture behaviors of ferroelectric/piezoelectric materials. J Intell Mater Sys Struc 16(7–8):673–687

Eastgate LO, Sethna JP, Rauscher M, Cretegny T (2002) Fracture in mode i using a conserved phase-field model. Phys Rev E71:036117

Francfort GA, Marigo J (1998) Revising brittle fracture as an energy minimization problem. J Mech Phys Solids 35(7):1319–1342

Hughes T (2000) The finite element method. Dover, Mineola, New York

Kamlah M (2001) Ferroelectric and ferroelastic piezoceramics—modeling of electromechanical hysteresis phenomena. Cont Mech Thermodyn 13:219–268

Kuhn C, Mueller R (2008) A phase field model for fracture. PAMM 8(1):10223–10224

Kuhn C, Mueller R, A continuum phase field model for fracture. Eng Fract Mech, (Special Issue on CMFD, submitted)

Mueller R, Gross D, Schrade D, Xu BX (2007) Phase field simulation of domain structure in ferroelectric materials within the context of inhomogeneity evolution. Int J Frac 147(1–4):173–180

Mueller R, Xu BX, Schrade D, Gross D Modelling of domain structure evolution in ferroelectric materials. Int J Fract, (Special Issue on IUTAM2009, accepted)

Schneider GA (2007) Influence of electric field and mechanical stresses on the fracture of ferroelectrics. Ann Rev Mater Res 37:491–538

Schrade D, Mueller R, Xu BX, Gross D (2007) Domain evolution in ferroelectric materials: a continuum phase field model and finite element implementation. Comput Meth Appl Mech Eng 196:4365–4374

Schrade D, Xu BX, Mueller R, Gross D (2009) On phase field simulations of ferroelectrics: Parameter identification and verification. Proceedings of the ASME 2008 smart materials, adaptive structures and intelligent systems (SMASIS2008), pp 301–308

Schrade D, Mueller R, Gross D (2010) Parameter identification in phase field models for ferroelectrics. Proc Appl Math Mech 9(1):369–370

Song YC, Soh AK, Ni Y (2007) Phase field simulation of crack tip domain switching in ferroelectrics. J Phys D Appl Phys 40:1175–1182

Spatschek R, Hartmann M, Brener EA, Mueller-Krumbhaar H (2006) Phase field modeling of fast crack propagation. Phys Rev Lett 96:015502

Xu BX, Schrade D, Mueller R, Gross D (2009) Micromechanical analysis of ferroelectric structures by a phase field method. Comput Mater Sci 45:832–836

Xu BX, Schrade D, Gross D, Mueller R (2010) Phase field simulation of domain structures in cracked ferroelectrics. Int J Fract. Special Issue: Broberg symposium. doi:10.1007/s10704-010-9471-z

Wang J, Zhang TY (2007) Simulations of polarization switching-induced toughening in ferroelectric ceramics. Acta Mate 55:2465–2477

Zhang TY, Zhao M, Tong P (2002) Fracture of piezoelectric ceramics. Adv Appl Mech 38:147–289

Zhang TY, Gao CF (2004) Fracture behaviors of piezoelectric materials. Theor Appl Frac Mech 41:339–379